

A METHODOLOGY FOR THE EMBEDDING OF SENSORS IN COMPONENTS MANUFACTURED USING METAL LASER POWDER BED FUSION

S.M. Uí Mhurchadha¹, M.P. Huynh^{1,2}, P.T. Quinn¹, I. Tomaz^{1,2}, R. Raghavendra^{1,2}

¹ SEAM Research Centre, School of Engineering, Waterford Institute of Technology, Ireland

² I-Form Advanced Manufacturing Research Centre, Ireland

Abstract

This paper presents a methodology for the embedding of a sensor in a 316L stainless steel component during the laser powder bed fusion process. The aim of this study is to overcome the drawbacks of traditional sensor attachment to the surface of a component via placing sensors into a part during the manufacturing process. A methodology for the embedding process that ensures the functionality of the sensor within the component is presented and a preliminary investigation into the effect of the embedding process on the manufactured part quality performed. An off-the-shelf accelerometer was embedded into a turbine and tested under rotational loading conditions. The interface microstructure where the print was stopped is also studied to investigate the effect of the sensor embedding methodology on material properties. The embedded sensor is capable of detecting off-axis rotation and over-speed of the turbine, two critical loading conditions that cause failure in turbines.

Keywords: *Smart components, experimental characterisation, 316L stainless steel, smart component*

Introduction

The integration of sensors into components allows for real-time monitoring of components and can be used to control the operating conditions of a system. Components with integrated sensors are referred to as “smart” components. With the development of Industry 4.0 [1], in-situ sensors can allow for the integration of a cyber-physical systems, allowing for automation and data exchange [2], which can transform industries, such as the automotive industry or allows for factories of the future, for example. To date, there are many applications of sensors integrated in a system either by adhesion to the surface of a component or in-line with a process. This means that often the required measurement at a location must be inferred from a sensor placed at a distance away from this point. Ideally, a sensor would be placed at this specific location; however, this often requires for the sensor to be embedded. Traditionally, for this to be achieved, material would have to be removed from the component to allow for access to adhere the sensor.

The freeform capability of additive manufacturing AM allows the inclusion of internal sensor housings that are uniquely accessible during the manufacturing process thanks to layer-by-layer nature of the process. Sensor embedding in an internal housing allows for measurements to be taken at a specific location, compared to inferred measurements from surface sensors. Furthermore, the sensor is protected from any external harsh environmental conditions.

Recent studies on the embedding of sensors in AM have focused on polymer materials [3–6] as well as metal AM components [7–10]. Hossain et al. [8] investigated the stop-go process. In this process, the manufacturing of a metal part was paused at a designed build height during the AM process; the sensor was placed in the pre-manufactured sensor housing, which was then placed into a pre-designed cavity in the part, and the printing process was resumed to complete the final part. This embedding method manufacturing process was also employed to investigate sensing capacity of an optical fibre that was embedded in a ceramic substrate [11]. The stop-go approach has a proven capability for integrating sensors for the production of functional parts; however, there are some shortcomings of the technique:

- There can be a gap between sensor housing and the remainder of the component.
- The melting temperature of metal is high (for example between 1450 and 1550 °C for 316L stainless steel), therefore, the sensor housing and insulation must be sufficient to protect it from heat and prevent melting of the sensor cover.
- The pausing of the AM process for the embedding of a sensor can lead to structural stress concentrations due to the disruption of the manufacturing process.

- The pre-design and manufacture of a housing to insulate sensor from the laser heat is not feasible for some applications.
- After a sensor is successfully embedded in a part, the sensor is inaccessible should it need to be replaced.

In this paper, an accelerometer is embedded into a 316L turbine part during the laser powder bed fusion (L-PBF) process using a stop-go methodology. The aim of this is to develop the production of a smart part, capable of monitoring loading conditions during operation and identify any critical loadings that will result in failure of the component. In the case of the turbine, these loading conditions include off-axis rotation (vibrations), potentially caused by a failed bearing, and over speed that can cause failure of the blades of the turbine. The smart AM turbine is tested using a custom test rig to investigate the functionality of the sensor to identify such loading conditions. Furthermore, the effect of the stop-go embedding process on the part quality is investigated. In particular, the interface hardness, porosity and microstructure are studied. The major advantage of the sensor being fully embedded in the part is that the sensor is placed at the centre of the part and therefore is ideally located to detect a failure before it causes damage elsewhere in the system due to debris, for example. However, the influence of the embedded sensor on rotor balance has not been investigated here, which required further research. The embedding of sensors internally can assist in the development of more accurate and responsive predictive maintenance plans with the aim to decrease a manufacturing processes downtime due to component failure. This will allow for the “smart” part to be replaced in the system in a timely and cost-effective manner.

Methodology

Design and manufacture of component

A turbine with an embedded accelerometer for the detection of off-axis rotation was chosen for this study. The turbine was designed for manufacture via L-PBF with minimal support structures to reduce post processing. The turbine included a sensor housing that was designed to allow for the embedding of an accelerometer at a particular height during the manufacturing process. The connections for the sensor were housed in the drive shaft coupling for the remaining duration of the L-PBF process. This allowed them to be easily accessed after the build. The component was also designed to be self-supporting i.e. no requirement for internal support structures within either of the housings. The turbine design with the sensor housing is presented in Figure 1 (a).

An off-the-shelf accelerometer (MPU-6050) with an integrated gyroscope was chosen for this initial embedding study due to its sensing capabilities, as well as its ability to withstand the chamber temperature during the build (80 °C). The sensor was embedded in epoxy resin using a FDM mould, as shown in Figure 1 (b), to protect it from the powder in the L-PBF process. The sensor and associated wiring were further insulated using Polytetrafluoroethylene (PTFE) tape to protect it from the elevated temperature of the AM process chamber.

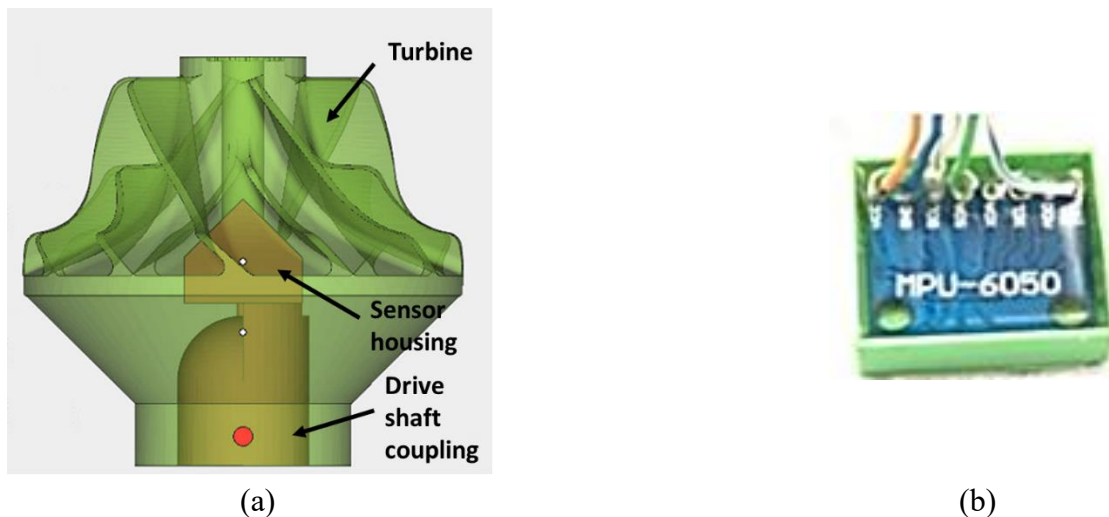


Figure 1. (a) The turbine design with the sensor and wiring housing for the embedding process, (b) the MPU-6050 sensor set in epoxy resin, using an FDM mould, prior to embedding in the L-PBF process.

The turbine, as shown in Figure 1, was manufactured using L-PBF in an EOS M280 machine. The material chosen for this was 316L stainless steel, supplied by Carpenter Additive [12]. The build plate was maintained at 80 °C during the build and embedding process. An inert Ar atmosphere was used in the chamber during L-PBF; however, the embedding process took place in air. The build was set up to automatically paused at the sensor insertion height and the build platform was moved downwards to avoid recoater crashing during the embedding process. This was timed so that the operator was present when the machine paused. The powder in both the sensor and the wiring housings was removed using a wet separator with a specially designed nozzle to allow for operation in the tight spacing within the housings, shown in Figure 2 (a). The sensor was then inserted into the empty housing, ensuring that the wires were located in the correct area of the housing to allow for access after the part was completed, as shown in Figure 2 (b). A new powder layer was recoated before restarting the build process to complete the manufacturing of the turbine. The embedding process took at total of 15 minutes before the flooding process to resume the build was started.

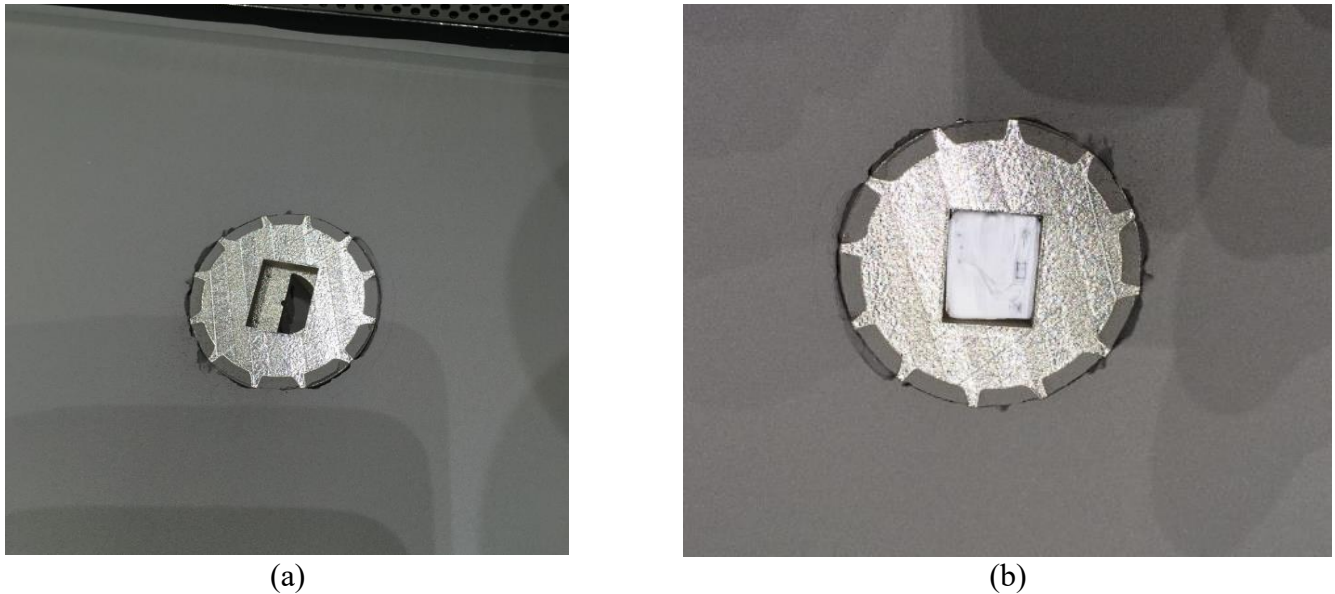


Figure 2. The sensor embedding process, showing (a) the sensor and wire housings after powder removal, and (b) the sensor (wrapped in PTFE tape) in the housing prior to continuing the L-PBF process.

Experimental validation of the embedded sensor

Prior to validation of the embedded sensor using a newly designed test rig, the sensor was non-destructively inspected using X-ray computed tomography (CT). A Phoenix V|tome|x L300 was employed to investigate any potential defects in the manufactured turbines and embedded sensors.

A test rig, as shown in Figure 3, was designed and manufactured to test the turbine under rotational loads. The turbine with the embedded sensor was attached to a hollow drive shaft with connection wires in the centre of the shaft. These connections wires were attached to a slip ring, allowing for the rotation of turbine to be decoupled from the data acquisition unit. The drive shaft was rotated using a brushed direct current geared motor. The drive shaft was held in the transverse direction using a two parallel rotational bearings, in line with the centreline of the shaft. This ensured that the only displacement on the turbine was the rotational velocity provided by the motor.

An Arduino Mega 260 was used for data acquisition from the embedded sensor. A calibration procedure for the definition of the x , y and z -axes within the code was run before each test. Acceleration in the x , y , and z -directions, as well as the temperature and the rotational angular velocity around the x , y and z -axes were measured. All measured data was written to a file. However, alternatively, this measured data could be used in real-time to drive the motor for a controlled feedback system. The key components to the custom made test rig and data acquisition system are presented in Figure 3.

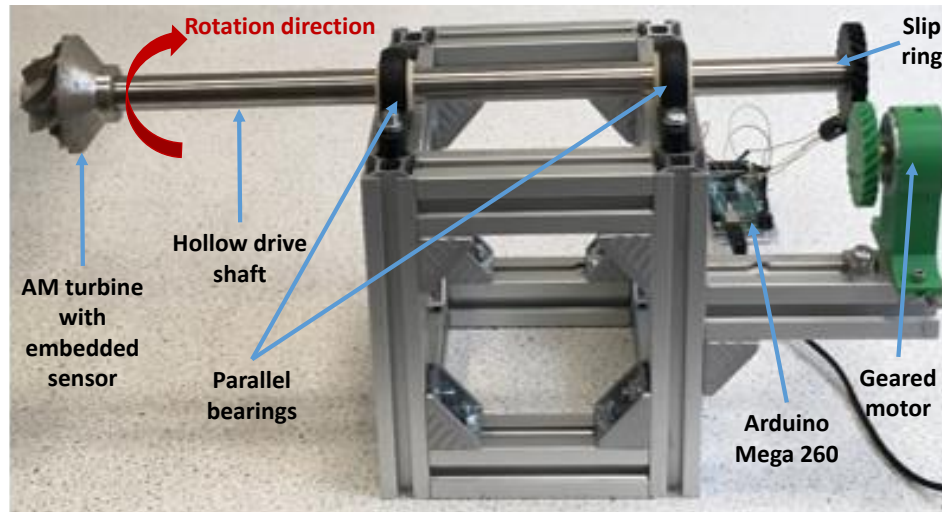


Figure 3. The turbine test rig, with the key components indicated.

Material characterisation

After the turbine with the embedded sensor was tested in the rig, it was sectioned using a Wire EDM (electrical discharge machine) to allow for cross-sectional analysis to take place using a Buehler ECOMET 30. This was aimed at investigation into the effect of the embedding process on the local porosity, as well as the micro-structural and mechanical properties of the component in the localised region affected by the paused build.

The sections of the turbine was mounted in epoxy resin and the surface perpendicular to the build direction was ground and polished to reveal any internal porosity. The polished cross-sections were imaged at 5 locations using a Keyence VH-Z 100R digital microscope at a magnification of x200. Images analysis in ImageJ software [13] was used to identify porosity in the cross-section.

The samples were then etched with Fry's reagent (150 ml H₂O, 50 ml HCL, 25 ml HNO₃, 1 g CuCl₂) for a time of approximately 30 s to reveal the microstructure, in particular the melt pools from the L-PBF process. Again, the etched cross-sections were imaged using a Keyence VH-Z 100R digital microscope at a magnification of x200.

Finally, the Vickers micro hardness of the region affected by the pausing of the build for the sensor embedding was measured. The micro-hardness was measured for 3 samples at multiple locations for (i) a distance 2.5 mm below the height for which the L-PBF process was paused, (ii) at the height the build was paused, and (iii) 2.5 mm above the height for which the L-PBF process was paused.

Results and discussion

Manufactured part

The completed turbine with the sensor successfully embedded is presented in Figure 4. No visual damage caused by the embedding process can be observed. The turbine was removed from the build plate without the requirement for the use of wire EDM.

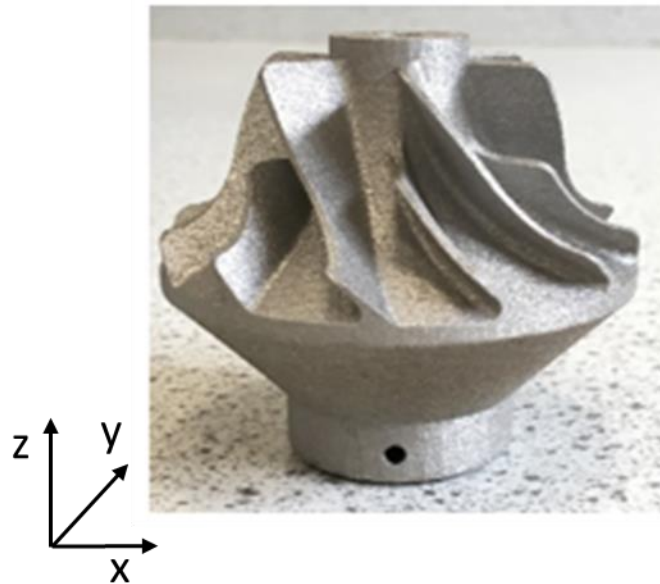


Figure 4. The manufactured part with embedded sensor.

Figure 5 presents X-ray CT imaging of the embedded sensor in the turbine. It can be seen from Figure 5 (a) that, despite best efforts during the embedding process, the sensor was either placed at an angle within the sensor housing or moved from the intended location after the embedding process was complete. This may have occurred due to the excess space above the sensor that was designed to allow for the housing to be built without the need for support material. This issue is addressed in the design iteration discussed below by using a cover plate above the sensor, elevating the requirement for additional space above the sensor.

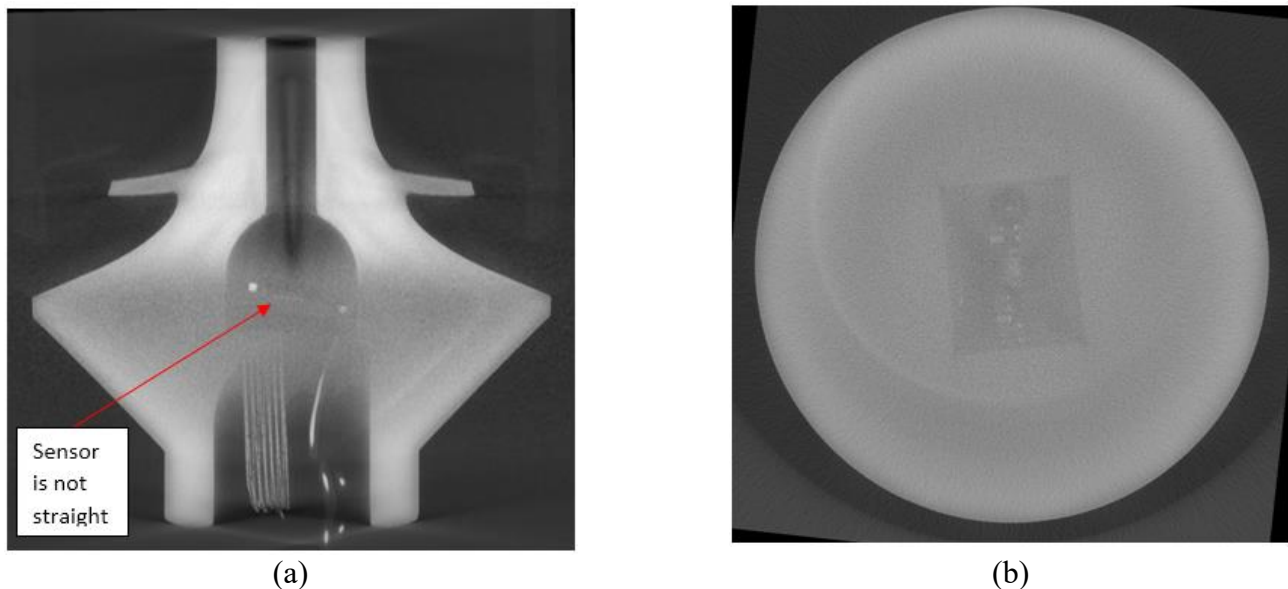


Figure 5. X-Ray CT images of the embedded sensor in the turbine in (a) the transverse direction, showing that the sensor moved after embedding, and (b) in the longitudinal direction.

Evaluation of the embedded sensor

Initial test results from the AM smart turbine are presented in Figures 6 and 7. These tests were completed at a constant applied rotational speed using the test rig shown in Figure 3. Figure 6 presents the x , y , and z -direction accelerations during rotation of the turbine at a RPM of 50. These acceleration readings can be integrated to get velocity and displacement [14], which would allow for monitoring of over-speed and off-axis rotation, respectively. There is fluctuation in the signal, which may be caused due to the sampling frequency. This can be

rectified by optimising the sampling frequency and incorporating a frequency filter to the signal. It was expected that the x and y-direction accelerations would be out of phase with each other by 90°. However, this was not the case. Also, a z-direction acceleration was observed, which should have been zero. This can be attributed to the off-axis location of the sensor within the turbine, as shown in Figure 5 (a). Figure 7 presents the gyroscope readings from the embedded sensor for the same test conditions as presented in Figure 6. These measurements can be used to monitor the rotational speed of the turbine in real-time operation. The primary axis of rotation is the z-axis; therefore, to allow investigation in vibration in the x and y-axes, the z-axis not shown in Figure 7. The presence of rotational measurements in the x and y-axes can be attributed to the off-axis location of the sensor within the turbine, as shown in Figure 5 (a).

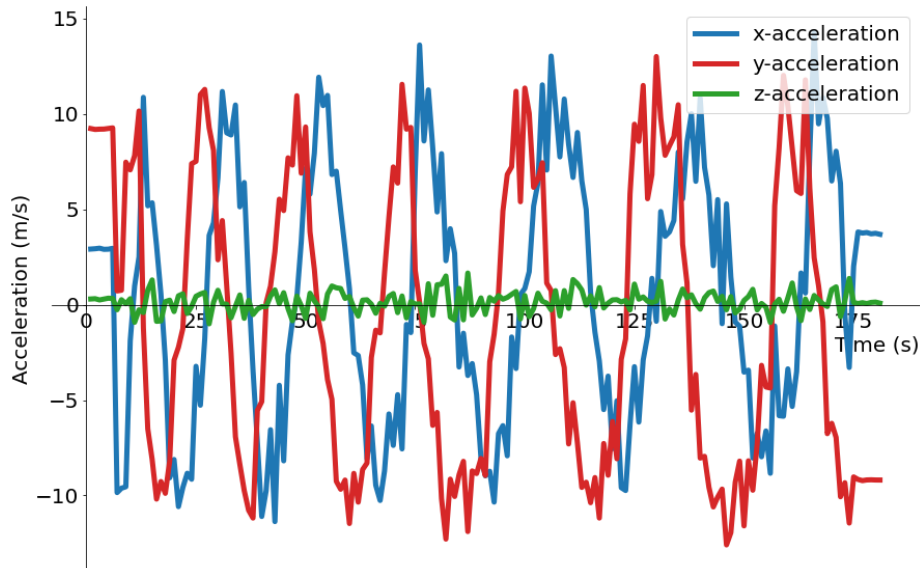


Figure 6. Acceleration measurements from the sensor in the x, y and z-directions.

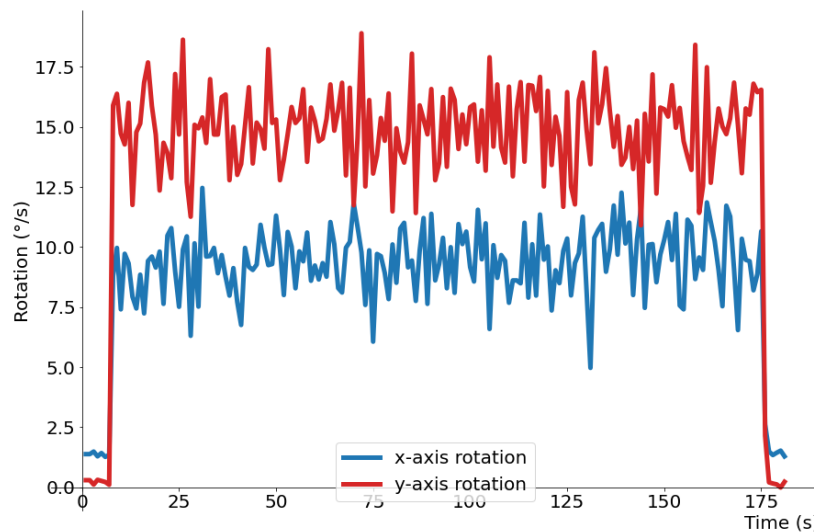


Figure 7. Rotational measurements from the sensor around the x and y-axes.

Effect of the embedding process on material characteristics

Figure 8 presents a comparison between the percentage density for the bulk part material and the interface region, which was affected by the pausing of the L-PBF process, for three samples cut from the turbine. The differences between the bulk material and the interface region is negligible. All locations have a density greater than 99.95%, which is within the specifications for the material [15]. No effect of the sensor embedding process on part density has been observed.

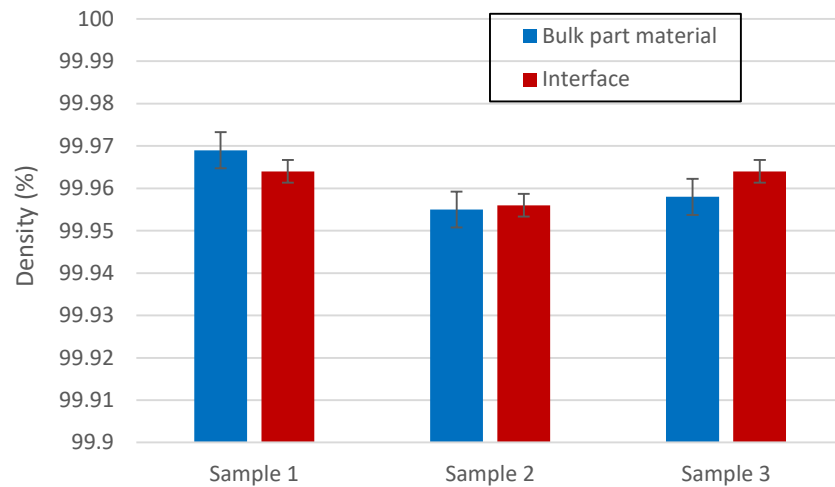


Figure 8. Density of the bulk material and in the interface region where the L-PBF process was paused, for 3 samples cut from the turbine.

An example of an etched cross-section in the build direction of one of the samples is presented in Figure 9. The melt pools of multiple layers can be seen. The interface region affected by the pausing of the L-PBF process is highlighted. In this region, the melt pools appear to be closer together. This is caused by the re-melting of layers when the print was resumed. Despite the build platform being maintained at a constant temperature during the embedding, the timing between successive layers changed significantly.

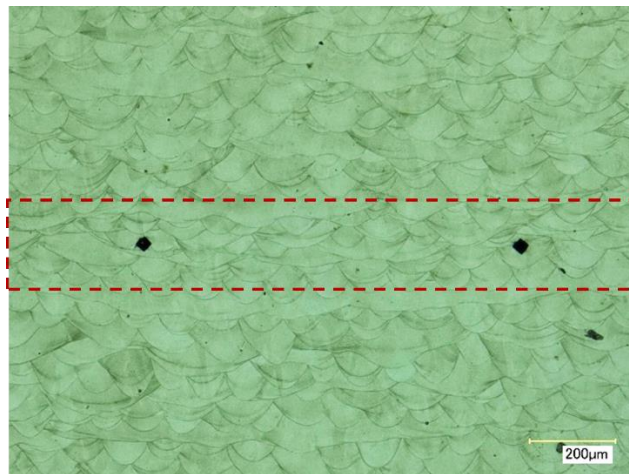


Figure 9. The etched cross-section, with the region affected by the pausing of the L-PBF process highlighted.

The Vickers hardness measurements at the build height at which the L-PBF was paused (interface), as well as at distances of 2.5 mm above and below this height, for 3 samples cut from the turbine are presented in Figure 10. The hardness in the interface region was 1.2 time higher than that of material unaffected by the L-PBF process pause for the embedding of the sensor.

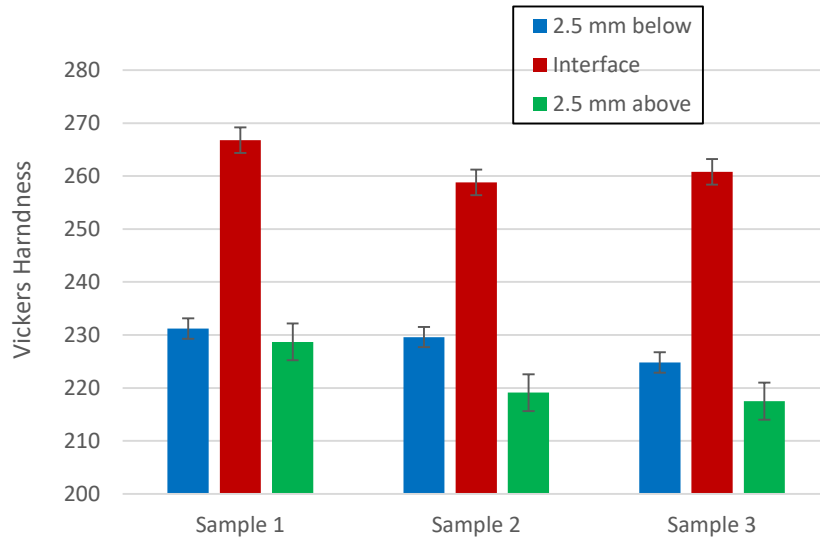


Figure 10. Vickers hardness measurements at the build height at which the L-PBF was paused, as well as at distances of 2.5 mm above and below this height, for 3 samples cut from the turbine.

Design iteration

Based on the results of the initial embedded sensor in the turbine, a design iteration has been made to ensure better a dimensional tolerance between the sensor and the component. For this design iteration, a cover plate was used to avoid the requirement to design the housing as a self-supporting structure, as proposed by Jung et al. [16]. This thickness of the cover plate was 0.5 mm to protect the sensor from the laser during exposure of the first layer after the embedding process is completed. A schematic of this design iteration is shown in Figure 11 (a) for a generic part with an embedded temperature sensor.

Figure 11 (b) presents an X-ray CT image of the successfully embedded temperature sensor in a 316L stainless steel part. It can be seen that no displacement of the sensor occurred, as happened with the turbine (shown in Figure 5). However, some distortion of this cover plate and lack of fusion between the plate and the top section of the part can be observed. Future work will further investigate this sensor embedding methodology and its effects on the material properties.

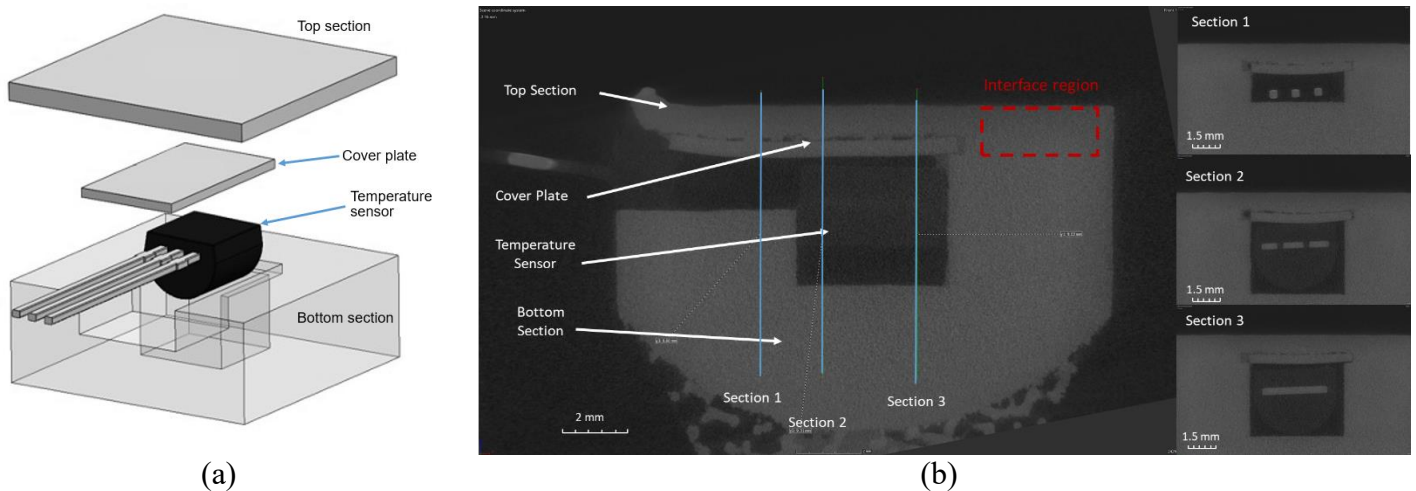


Figure 11. (a) Design iteration incorporating a cover plate to allow for better dimensional tolerance between the sensor and the component, and (b) X-Ray CT image of an embedded temperature sensor using this methodology.

Conclusions

This paper has presented a methodology for the embedding of an accelerometer sensor in a 316L stainless steel turbine during the laser powder bed fusion process. A stop-go method, in which the L-PBF process was paused to embed the sensor in a sensor housing in the turbine at a particular height before resuming the L-PBF process to complete the manufacture of the turbine. The sensor was validated using a custom made test rig and the effect of this process on the material characteristics was investigated. A design iteration incorporating a cover plate for more accurate placement of the sensor was also investigated. The findings of this paper can be concluded as follows:

- Non-destructive testing via X-Ray CT imaging showed that the sensor moved from the desired location. This was due to the excess space above the sensor in the housing, designed to ensure that the housing was self-supporting during the manufacturing via L-PBF. The location of the sensor caused for some off-axis rotation to be observed during testing of the turbine.
- There was no effect of the embedding process on the material density at the location where the L-PBF process was paused. However, finer grain size and closer melt pools in the build direction were observed in this region.
- Vickers micro-hardness measurements location where the L-PBF process was paused and resumed were approximately 1.2 times higher compared to the bulk material of the turbine. This may be due to formation of finer grains in this region during the re-melting process when the L-PBF process resumed.

Finally, a design iteration incorporating a cover plate for the sensor was investigated. This resulted in better control of positioning of the sensor in the housing. However, lack-of-fusion between the cover plate and subsequent L-PBF layers was observed. This methodology will be further investigated. Also, the use of wireless, fully-embedded sensors will be investigated in future work.

Acknowledgements

This publication has emanated from research supported in part by a research grant from Science Foundation Ireland (SFI) under Grant Number 16/RC/3872 and is co-funded under the European Regional Development Fund. The authors also wish to acknowledge the support of 3DWIT for the use of their AM equipment and Wire EDM.

References

- [1] H. Gupta, A. Kumar, P. Wasan, Industry 4.0, cleaner production and circular economy: An integrative framework for evaluating ethical and sustainable business performance of manufacturing organizations, *Journal of Cleaner Production*, 295 (2021). <https://doi.org/10.1016/j.jclepro.2021.126253>
- [2] J. Downey, P. O'Leary, R. Raghavendra, Comparison and analysis of audible sound energy emissions during single point machining of HSTS with PVD TiCN cutter insert across full tool life, *Wear*, 313 (2014) 53-62. <https://doi.org/10.1016/j.wear.2014.02.004>
- [3] R.R.J. Maier, W.N. MacPherson, J.S. Barton, M. Carne, M. Swan, J.N. Sharma, S.K. Futter, D.A. Knox, B.J.S. Jones, S. McCulloch, Embedded Fiber Optic Sensors Within Additive Layer Manufactured Components, *IEEE Sens. J.* 13 (2013) 969–979. <https://doi.org/10.1109/JSEN.2012.2226574>.
- [4] A. Leal-Junior, J. Casas, C. Marques, M. Pontes, A. Frizera, Application of Additive Layer Manufacturing Technique on the Development of High Sensitive Fiber Bragg Grating Temperature Sensors, *Sensors*. 18 (2018) 4120. <https://doi.org/10.3390/s18124120>.
- [5] M. Sajid, J.Z. Gul, S.W. Kim, H.B. Kim, K.H. Na, K.H. Choi, Development of 3D-Printed Embedded Temperature Sensor for Both Terrestrial and Aquatic Environmental Monitoring Robots, *3D Print. Addit. Manuf.* 5 (2018) 160–169. <https://doi.org/10.1089/3dp.2017.0092>.
- [6] L. Fang, T. Chen, R. Li, S. Liu, Application of Embedded Fiber Bragg Grating (FBG) Sensors in Monitoring Health to 3D Printing Structures, *IEEE Sens. J.* 16 (2016) 6604–6610. <https://doi.org/10.1109/JSEN.2016.2584141>.

- [7] P. Stoll, B. Leutenecker-Twelsiek, A. Spierings, C. Klahn, K. Wegener, Temperature Monitoring of an SLM Part with Embedded Sensor, in: *Ind. Addit. Manuf. - Proc. Addit. Manuf. Prod. Appl. - AMPA2017*, Springer International Publishing, Cham, 2018: pp. 273–284. https://doi.org/10.1007/978-3-319-66866-6_26.
- [8] M.S. Hossain, J.A. Gonzalez, R.M. Hernandez, M.A.I. Shuvo, J. Mireles, A. Choudhuri, Y. Lin, R.B. Wicker, Fabrication of smart parts using powder bed fusion additive manufacturing technology, *Addit. Manuf.* 10 (2016) 58–66. <https://doi.org/10.1016/j.addma.2016.01.001>.
- [9] D. Havermann, J. Mathew, W.N. MacPherson, D.P. Hand, R.R.J. Maier, Measuring residual stresses in metallic components manufactured with fibre Bragg gratings embedded by selective laser melting, in: H.J. Kalinowski, J.L. Fabris, W.J. Bock (Eds.), 2015: p. 96340T. <https://doi.org/10.1117/12.2194352>.
- [10] R.R.J. Maier, D. Havermann, O. Schneller, J. Mathew, D. Polyzos, W.N. MacPherson, D.P. Hand, Optical fibre sensing in metals by embedment in 3D printed metallic structures, in: J.M. López-Higuera, J.D.C. Jones, M. López-Amo, J.L. Santos (Eds.), 2014: p. 915707. <https://doi.org/10.1117/12.2064886>.
- [11] S. Srivastava, R.K. Garg, V.S. Sharma, N.G. Alba-Baena, A. Sachdeva, R. Chand, S. Singh, Multi-physics continuum modelling approaches for metal powder additive manufacturing: a review, *Rapid Prototyp. J.* 26 (2020) 737–764. <https://doi.org/10.1108/RPJ-07-2019-0189>.
- [12] Carpenter Additive, Technical Data Sheet CT PowderRange 316L F, n.d.
- [13] M.D. Abràmoff, P.J. Magalhães, S.J. Ram, Image Processing with ImageJ, Biophotonics International, A Laurin Publication https://imagej.nih.gov/ij/docs/pdfs/Image_Processing_with_ImageJ.pdf, n.d.
- [14] InvenSense Inc. MPU-6000 and MPU-6050 Product Specification Revision 3.4, 2013
- [15] EOS Material data sheet EOS Stainless Steel 316L for EOS M 280, EOS GmbH - Electro Opt. Syst. (2014). <https://cdn1.scrvt.com/eos/77d285f20ed6ae89/dd6850c010d3/EOSStainlessSteel316L.pdf>.
- [16] I.D. Jung, M.S. Lee, J. Lee, H. Sung, J. Choe, H.J. Son, J. Yun, K.T.K. Kim, M. Kim, S.W. Lee, S. Yang, S.K. Moon, K.T.K. Kim, J.-H. Yu, Embedding sensors using selective laser melting for self-cognitive metal parts, *Addit. Manuf.* 33 (2020) 101151. <https://doi.org/10.1016/j.addma.2020.101151>.